

A simple model of ozone-temperature coupling in the tropical lower stratosphere

William J. Randel^{1,2}, Fei Wu¹, Alison Ming³, Peter Hitchcock⁴

5

¹National Center for Atmospheric Research, Boulder, CO, USA

²COSMIC Program, University Corporation for Atmospheric Research, Boulder, CO, USA

³University of Cambridge, Cambridge, UK

⁴Cornell University, Ithaca, NY

10 *Correspondence to:* William Randel (randel@ucar.edu)

Abstract. Observations show strong correlations between large-scale ozone and temperature variations in the tropical lower stratosphere across a wide range of time scales. We quantify this behavior using monthly records of ozone and temperature data from SHADOZ tropical balloon measurements (1998-2016), along with global satellite data from Aura MLS and GPS radio occultation over 2004-2018. The observational data demonstrate strong in-phase ozone-temperature coherence
15 spanning sub-seasonal, annual and interannual time scales, and the slope of the temperature-ozone relationship (T/O3) varies as a function of time scale and altitude. We compare the observations to idealized calculations based on the coupled zonal mean thermodynamic and ozone continuity equations, including ozone radiative feedbacks on temperature, where both temperature and ozone respond in a coupled manner to variations in the tropical upwelling Brewer-Dobson circulation. These calculations can approximately explain the observed (T/O3) amplitude and phase relationships, including sensitivity to
20 time scale and altitude, and highlight distinct balances for ‘fast’ variations (periods < 150 days, controlled by transport across background vertical gradients) and ‘slow’ coupling (seasonal and interannual variations, controlled by radiative balances).

1 Introduction

Large-scale ozone and temperature variations in the tropical lower stratosphere exhibit strong correlations across a range of time scales. This behavior is well-known for the annual cycle in the lower stratosphere (Chae and Sherwood, 2007; Randel et al, 2007) and for interannual variations linked to the quasi-biennial oscillation (QBO) (e.g. Hasebe et al, 1994; Baldwin et al, 2001; Witte et al, 2008; Hauchecorne et al, 2010) and El Nino Southern Oscillation (ENSO; Randel et al, 2009). Abalos et al (2012; 2013) and Gilford et al (2016) also note strong temperature-ozone correlations in this region across a range of time scales. Calculations have shown that the radiative effects of ozone feed back onto and enhance temperature variations, and this topic has been well-studied as related to the annual cycle in the tropical lower stratosphere

30 (Chae and Sherwood, 2007; Fueglistaler et al, 2011; Ming et al, 2017; Gilford and Solomon, 2017), and also by Forster et al
(2007) and Polvani and Solomon (2012) for decadal-scale trends. Yook et al (2020) showed that ozone feedback is an
important contribution to tropical stratospheric thermal variability in global models. Birner and Charlesworth (2017) and
Dacie et al (2019) have demonstrated strong sensitivity of tropical stratospheric temperatures to ozone using idealized one-
dimensional model calculations, following the earlier results of Thuburn and Craig (2002). Charlesworth et al (2019)
35 extended that work to study transient ozone-temperature feedbacks, highlighting larger effects for low frequency variations
(periods longer than about half a year).

The dominant mechanism for strong ozone-temperature correlations in the tropical lower stratosphere is relatively
simple, namely, variations in upwelling (i.e. fluctuations in the tropical Brewer-Dobson circulation) acting on the strong
background vertical gradients of both ozone and potential temperature, leading to correlated variability. This behavior was
40 quantified from observations and model simulations in Abalos et al (2012; 2013), highlighting the control of upwelling for
forcing transient variations in temperature, ozone and other trace species with strong vertical gradients, such as carbon
monoxide (CO). The radiative feedback of ozone to temperature imparts further complexity to this simple system, and that is
the focus of this work. Here we update the observational evidence of ozone-temperature coupling based on long records of
tropical balloon measurements from SHADOZ (Thompson et al, 2003), focusing on annual and interannual variability. We
45 also analyze over a decade of continuous satellite measurements to quantify ozone-temperature coherence and phase in the
tropical stratosphere over a continuous range of time scales. We compare the observational results with calculations based on
the coupled zonal mean thermodynamic and ozone continuity equations, simplified to approximate the balances in the
tropical lower stratosphere, and including ozone feedback on temperature. Our goal is to explain the salient features of
temperature-ozone (T-O3) coupling from observations in a relatively simple framework, including the frequency and altitude
50 dependences of the (T/O3) amplitude and phase relationships. These results are a complement to the recent analyses of
Birner and Charlesworth (2017) and Charlesworth et al (2019), based on a very different model.

2 Data and Analyses

2.1 SHADOZ ozone and temperature

The Southern Hemisphere Additional Ozonesonde (SHADOZ) network consists of ~12 stations covering a range of
55 longitudes over the latitude band $\sim 10^\circ \text{ N} - 20^\circ \text{ S}$, with measurements beginning in 1998 (Thompson et al, 2003). Recent
reprocessing of the data is discussed in Witte et al (2017) and Thompson et al (2017). The SHADOZ balloons measure
ozone and pressure-temperature-wind profiles, with effective vertical resolution of $\sim 50\text{-}100\text{m}$. The data used here are
sampled with 0.5 km vertical spacing, and we focus on altitudes 15-30 km. We analyze data from SHADOZ stations with
long and continuous records, updated from Randel and Thompson (2011). There are typically 2-4 observations per month at
60 each of the SHADOZ stations, which we combine into simple monthly averages. The stratospheric segment of the ozone
profile exhibits a high degree of longitudinal symmetry (Thompson et al, 2003; Randel et al, 2007; Randel and Thompson,

2011) and we combine monthly average results from all stations to provide approximate zonal average monthly means of ozone and temperature, with data covering 1998-2016.

2.2 Aura MLS ozone and GPS temperature

65 Satellite ozone measurements from the Aura Microwave Limb Sounder (MLS) are analyzed for the period
September 2004 – May 2018. We use retrieval version 4.2 (Livesey et al, 2018). Data are available for standard pressure
levels (12 per decade) covering 316 hPa to above 1 hPa; the vertical resolution of the grid is ~ 1.3 km, but the resolution of
the MLS measurements is closer to ~ 3 km (i.e. the data are oversampled). Data quality for MLS v4.2 ozone is discussed in
Livesey et al (2018). Our analyses focus on the latitude band 10° N-S, and we calculate zonal mean values for 5-day (pentad)
70 averages. Some isolated data gaps are filled by linear interpolation in time. This provides a long, continuous time series of
MLS ozone covering 998 pentads (4990 days).

Temperature data are obtained from GPS radio occultation, which provides high quality and high vertical resolution
(~ 1 km) measurements over 10-30 km, and near-global sampling (Anthes et al, 2008). We combine measurements from
several different GPS satellites for the period overlapping the MLS ozone data (September 2004 – May 2018), and construct
75 pentad time series from data over 10° N-S to match the MLS ozone time series discussed above. We focus on altitude levels
close to the MLS ozone grid. The time series analyzed here are an update of the data analyzed in Randel and Wu (2015), and
further details are discussed there.

2.3 Spectrum analysis

We include spectrum and cross-spectrum analysis of the satellite-derived ozone and temperature time series to
80 quantify frequency-dependent relationships. Spectra are calculated by direct Fourier transform of the 998-pentad time series
for both ozone and temperature, resolving periods of 4990 to 10 days, with a frequency resolution of $\Delta\omega = (2\pi/4990)$ days).
Calculations are based on standard formulas in Jenkins and Watts (1968). Power spectra are smoothed with a Gaussian-
shaped smoothing window with half-width $2\Delta\omega$. Temperature-ozone amplitude ratios, coherence squared and phase spectra
are calculated using a wider bandwidth ($10\Delta\omega$) to enhance statistical stability. This results in approximately 10 independent
85 Fourier harmonics for each spectral estimate, and the resulting 95% significance level for the coh2 statistic is 0.45. The high-
and low-frequency ends of the spectra are smoothed using one-sided Gaussian smoothing so that significance levels are
somewhat higher.

3 Simplified zonal mean theory

3.1 Coupled thermodynamic and ozone continuity equations

90 We explore the coupling of ozone and temperature based on the zonal mean thermodynamic and ozone continuity equations, simplified to approximate behavior in the tropical lower stratosphere, namely neglecting mean meridional advection and eddy forcing terms. The zonal mean thermodynamic equation in transformed Eulerian-mean coordinates, using a log-pressure vertical coordinate (Andrews et al, 1987) is:

$$\partial T / \partial t = -v^*(\partial T / \partial y) - w^*S + \text{eddy terms} + Q \quad (1)$$

95 Here T is zonally averaged temperature, (v^*, w^*) are components of the residual meridional circulation, S is a stability parameter, and Q is the zonal mean diabatic heating rate. We note that all variables in the equations are zonal mean quantities, but no overbars are used in the notation. In the tropical lower stratosphere the v^* and eddy forcing terms are relatively small (Abalos et al, 2013), so that the approximate thermodynamic balance is:

$$\partial T / \partial t = -w^*S + Q \quad (2)$$

100 In this work we specify the zonal mean diabatic forcing Q with two components $Q = Q_{\text{relaxation}} + Q_{\text{ozone}}$, representing radiative relaxation and ozone forcing of temperature, respectively. We assume radiative relaxation is proportional to temperature, $Q_{\text{relaxation}} = -\alpha (T - T_{\text{eq}})$, with T_{eq} an equilibrium temperature and α an inverse radiative damping time scale (Andrews et al, 1987; Hitchcock et al, 2010). α is obtained from the results of Hitchcock et al (2010) as discussed below. In addition, correlated variations in ozone produce a positive radiative feedback on temperature (e.g. Fueglistaler et al, 2011; Gilford et al, 2017; Ming et al, 2017), and while this is in general a non-local effect (in altitude), for simplicity we model the temperature tendency as proportional to the local ozone anomaly: $Q_{\text{ozone}} = \beta (X - X_{\text{eq}})$. Here X is zonal mean ozone mixing ratio, X_{eq} is a background equilibrium ozone value and β is a constant derived from radiative transfer calculations (described below). Based on these simplified assumptions, the zonal mean thermodynamic equation becomes:

$$\partial T / \partial t = -w^*S - \alpha (T - T_{\text{eq}}) + \beta (X - X_{\text{eq}}) \quad (3)$$

110 Assuming harmonic time expansions of the form $T(t) = \sum T_{\sigma} \exp^{i\sigma t}$, with σ the angular frequency ($2\pi/\text{period}$), and likewise for $w^*(t)$ and $X(t)$, and assuming T_{eq} , X_{eq} and S are constant in time, Eq. 3 can be rewritten as an equation for each harmonic component:

$$i\sigma T_{\sigma} = -w^*_{\sigma} S - \alpha T_{\sigma} + \beta X_{\sigma} \quad (4)$$

A similar analysis is applied to the zonal mean ozone continuity equation (Andrews et al, 1987, Eq. 9.4.13):

115
$$\partial X / \partial t = -v^*(\partial X / \partial y) - w^*(\partial X / \partial z) + \text{eddy terms} + P - L \quad (5)$$

Here $P-L$ represents chemical ozone production minus loss terms. In contrast to the thermodynamic balance discussed above, the eddy terms for ozone transport in the tropical lower stratosphere are not negligible, and there is a maximum during boreal summer near the tropopause related to transport from the subtropical monsoon circulations (Konopka et al, 2009, 2010;

Abalos et al, 2013). This contribution is relatively large below ~80 hPa (18 km). However, for simplicity in our idealized
 120 calculations the eddy terms are neglected here, along with the w^* term. This yields:

$$\partial X/\partial t = -w^* X_z + P - L, \quad (6)$$

where we have defined $X_z = (\partial X/\partial z)$. In the tropical lower stratosphere ozone production minus loss is positive and is
 relatively constant in time, with a small semi-annual variation in production following solar inclination (Abalos et al, 2013).
 We parameterize ozone loss as $L = -\delta (X - X_{eq})$, where δ is the inverse lifetime of ozone, obtained from model calculations as
 125 described below. Assuming a constant production rate (P) and a constant background ozone gradient X_z , the harmonic
 expansion of Eq. 6 is then given by the simple balance:

$$i\sigma X_\sigma = -w^*_\sigma X_z - \delta X_\sigma \quad (7)$$

We show idealized model calculations below including realistic ozone damping estimates (along with results for no
 damping), which demonstrate that ozone damping has a relatively small influence for the majority of results.

130 The balances in the simplified equations (Eq. 4 and 7) are driven by temperature and ozone responses to imposed
 vertical velocity variations (w^*) in the tropical lower stratosphere, as is observed and derived from model simulations
 (Abalos et al, 2012; 2013). Temperature is furthermore influenced by radiative damping (α term) and the radiative response
 to ozone changes (β term), while ozone balance includes damping (δ term). Equations 4 and 7 can be combined to eliminate
 the w^*_σ dependence to obtain a single equation relating temperature and ozone harmonic components, in particular the
 135 temperature/ozone ratio as a function of frequency:

$$(T_\sigma/X_\sigma) = (S/X_z) (i\sigma + (\beta' + \delta))/(i\sigma + \alpha), \quad (8)$$

with $\beta' = (X_z/S) \beta$. This can be rewritten as:

$$(T_\sigma/X_\sigma) = A + iB$$

$$\text{with } A = (S/X_z) (\sigma^2 + \alpha(\beta' + \delta))/(\sigma^2 + \alpha^2)$$

$$\text{and } B = (S/X_z) \sigma(\alpha - (\beta' + \delta))/(\sigma^2 + \alpha^2)$$

140 Here (S/X_z) is a key parameter related to the ratio of background stability (potential temperature gradient) to ozone vertical
 gradient, which is derived directly from the time average temperature and ozone profile data; the vertical profile of (S/X_z) is
 shown in Fig. 1c. We note some small (~10%) seasonal and interannual variations to the individual S and X_z terms in the
 tropical lower stratosphere, but these follow each other and the ratio (S/X_z) is more nearly constant. Equation 8 can be
 145 rewritten as expressions for (T_σ/X_σ) amplitude and phase:

$$(T_\sigma/X_\sigma)_{\text{amplitude}} = \text{sqrt}(A^2 + B^2) \quad (9a)$$

$$(T_\sigma/X_\sigma)_{\text{phase}} = \tan^{-1}(B/A) \quad (9b)$$

Our analyses focus on evaluating the quantity (T_σ/X_σ) as a metric for temperature sensitivity to ozone as a function of
 frequency (and altitude), and below we test results from this idealized model with (T_σ/X_σ) amplitude and phase derived from
 150 observations. We note that the phase is defined such that positive values denote temperature variations leading ozone in time.

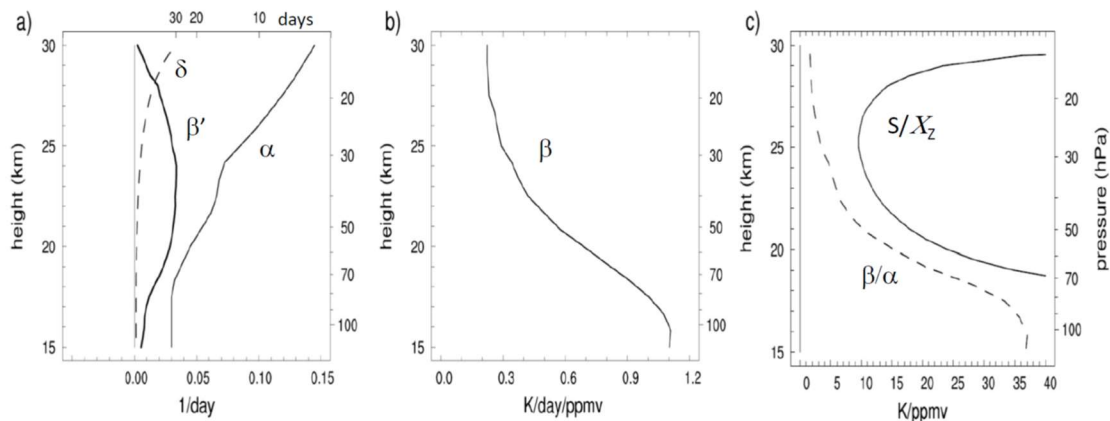
The observational data are based on measurements from SHADOZ and MLS/GPS in the deep tropics over $\sim 10^\circ$ N-S, and hence represent this tropical average. We note that Stolarski et al (2014) and Tweedy et al (2017) highlight distinct ozone behavior in southern tropics vs. northern tropics in the region up to ~ 18 km, due to influence of the boreal summer monsoons. This could potentially impact our comparisons close to the tropopause, but should have less influence above ~ 18 km.

The (T_σ/X_σ) ratio in Eq. 8 is a generally complex function of σ , α , β' , δ and (S/X_z) , but it is useful to consider the high- and low-frequency limits (compared to the inverse time scales α and $(\beta'+\delta)$). For high frequencies ($\sigma \gg \alpha, (\beta'+\delta)$), the (T_σ/X_σ) ratio simplifies to $\sim (S/X_z)$, i.e. the temperature and ozone anomalies are in phase, with a ratio simply related to the background gradients in potential temperature and ozone. For the low frequency limit ($\sigma \ll \alpha, (\beta'+\delta)$), $(T_\sigma/X_\sigma) \sim (S/X_z) ((\beta'+\delta)/\alpha)$. For δ smaller than β' (as suggested by Fig. 1a), the ratio simplifies to (β'/α) . This expresses an in-phase balance of ozone and temperature associated with the α and β radiative terms in the thermodynamic equation (Eq. 3), i.e. heating from ozone anomalies balances radiative cooling. The simple model predicts that the lower frequency limit will occur for frequencies lower than $(\beta'+\delta)$, corresponding to periods longer than about 200 days at 24 km (using the values in Fig. 1a).

The effect of ozone feedback on temperature is given by the β term in Eq. 3, quantified by the β' term in the coupled equations (Eq. 8). Below we directly evaluate this influence by comparing calculations with $\beta'=0$, which explicitly quantifies the ozone feedback on temperature in our simplified framework. The simple model suggests this influence will be seen at low frequencies; in the absence of ozone feedback the (T_σ/X_σ) low frequency limit reduces to $(S/X_z) (\delta/\alpha)$.

3.2 Estimating α , β and δ from model calculations

Our calculations use a vertical profile of α in the tropical stratosphere derived by Hitchcock et al (2010), as shown in Fig. 1a. These results are based on regressions derived from radiative heating rates and temperatures output from a chemistry-climate model. We note that there are several uncertainties inherent in these calculations, including factors such as tropospheric clouds influencing lower stratospheric heating rates and dependence on the vertical scale of temperature perturbations (Hartmann et al, 2001; Hitchcock et al, 2010). The overall structure and magnitude of α used here is consistent with other published estimates, e.g. Newman and Rosenfield (1997) and Randel and Wu (2015).



175

Figure 1. Vertical profiles of parameters used in the theoretical model calculations. (a) α , β' and δ , b) β and c) (S/X_z) and (β/α) . The top axis in (a) shows the associated time scales in days.

We estimate vertical profiles of the parameter β from radiative transfer calculations using a modified version of the
 180 Morcrette (1991) radiation scheme (Zhong and Haigh, 1995). The calculations use realistic background temperature, ozone
 and water vapor profiles, and carbon dioxide is assumed to be well mixed with a volume mixing ratio of 360 ppmv.
 Shortwave heating rates are calculated as diurnal averages, including realistic surface albedo, and all calculations assume
 clear-sky conditions. β is derived by applying a 0.1 ppmv perturbation to the ozone field at each vertical level, and
 calculating the ratio of the instantaneous heating rate change at that level to the amplitude of the ozone perturbation. The
 185 resulting profile of β is shown in Fig. 1b, with typical values of 0.3-1.0 (K/day/ppmv), decreasing in altitude away from the
 tropopause. The vertical structure of $\beta' = (X_z/S) \beta$ is included in Fig. 1a, showing a magnitude somewhat smaller than α
 throughout the profile. This in turn implies a positive $(T_\sigma/X_\sigma)_{\text{phase}}$ from Eqns. 8-9b (including a realistic small δ), i.e.
 temperature leads ozone in the coupled response based on these parameters, although as shown below the phase difference
 turns out to be small. Vertical profile of the quantity (β/α) (zero frequency limit for (T_σ/X_σ) , for small δ) is included in Fig.
 190 1c, showing decrease from the tropopause to the middle stratosphere with values substantially smaller than (S/X_z) .

We derived an estimate of the damping rate $\delta(z)$ for ozone from simulations of the Whole Atmosphere Community
 Climate Model (WACCM; Marsh et al, 2013), which includes a sophisticated stratospheric ozone chemical scheme. These
 calculations use daily zonal average output of ozone amount (X) and photochemical ozone loss rate (L) as a function of
 latitude and altitude, and we take an annual average of their ratio: $\delta(z) = (L/X)$, averaging results over 10° N-S. The
 195 resulting vertical profile of δ is shown in Fig. 1a, showing very small damping (long ozone lifetimes) in the lower
 stratosphere, increasing to slightly larger values in the middle stratosphere (damping time scale of ~30 days at 30 km).
 Calculations below show idealized model results including these realistic values of δ , and for comparison we also include
 results for $\delta=0$. Including realistic values of ozone damping has almost no influence on calculations in the lower stratosphere

because of the very small damping. Damping can have a small but noticeable effect at higher altitudes for lower frequency variations (increasing the T_{σ}/X_{σ} ratios), but still only accounts for $\sim 10\%$ effect.

4 Ozone and temperature observations

4.1 Annual and QBO variability in SHADOZ ozone and temperature

The approximately monthly sampling of SHADOZ data allows characterization of the annual cycle and interannual variations of tropical stratospheric ozone and temperature. There is a relatively large annual cycle in ozone and temperature in the tropical lower stratosphere over $\sim 16\text{-}22$ km, with relative maxima during boreal summer and temperature slightly leading ozone in time. Figure 2 shows this behavior for the 19 km level, near the peak of the annual cycle. This correlated ozone-temperature behavior is mainly a response to the annual cycle in tropical upwelling (Randel et al, 2007); horizontal transport from the boreal summer monsoons also contributes to the seasonal maximum in ozone close to the tropopause (Konopka et al, 2009, 2010; Stolarski et al, 2014; Tweedy et al, 2017), but mean upwelling is the dominant mechanism above 18 km (Abalos et al, 2013). Above 23 km the annual cycle becomes small and the dominant seasonal variation becomes semi-annual in both ozone and temperature. We note that the seasonal variations in Fig. 2 are very similar based on the MLS ozone and GPS temperature data (not shown).

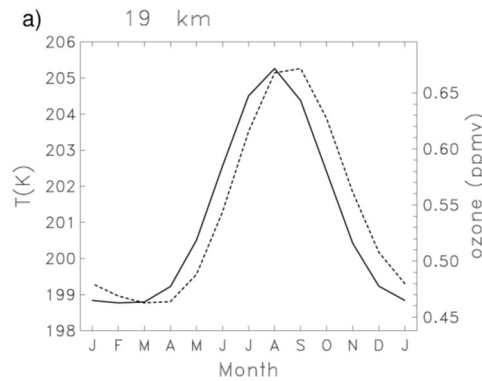


Figure 2. Climatological annual cycles of ozone and temperature at 19 km derived from SHADOZ measurements over 1998-2016.

215

Interannual anomalies in ozone and temperature from SHADOZ data over 1998-2016 are shown in Fig. 3, derived by simply subtracting the mean annual cycle. In Fig. 3 ozone anomalies are shown in terms of ozone density (DU/km) instead of mixing ratio, in order to emphasize variations throughout the lower stratosphere. As is well known, there are strong downward propagating anomalies in ozone and temperature linked to the QBO; the ozone and temperature anomalies are approximately in phase over $\sim 17\text{-}27$ km, and the variations in ozone are small above 27 km due to a transition from dynamical control in the lower stratosphere to photochemical control above ~ 27 km (e.g. Chipperfield and Gray, 1992; Park et al, 2017). Episodic ENSO events also result in correlated ozone-temperature variations in the tropical lower stratosphere,

for levels from the tropopause to ~22 km (Randel et al, 2009; Calvo et al, 2010). The constructive interference of QBO and ENSO effects can result in large anomalies near and above the tropopause (e.g. Diallo et al, 2018), as seen for the SHADOZ data in 1999-2000 and 2015-2016.

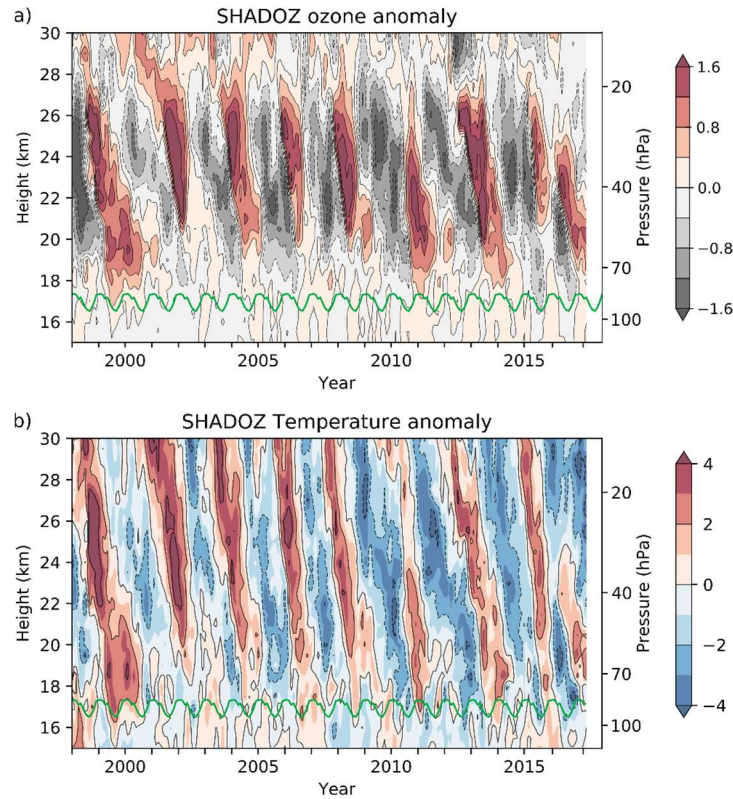
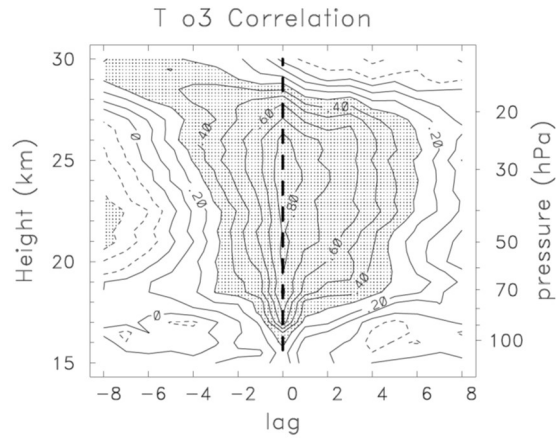


Figure 3. Height-time sections of deseasonalized anomalies in (a) ozone and (b) temperature (K) from SHADOZ data. Ozone anomalies are expressed in terms of ozone density (DU/km) to emphasize variability throughout the lower stratosphere. The green lines denote the cold point tropopause.

230

Figure 4 shows the ozone-temperature correlation derived from the deseasonalized SHADOZ data (from Fig. 3) as a function of altitude and time lag. Strong positive correlations (>0.8) are found over 17-27 km, as expected from Fig. 3. The strongest correlations occur near zero time lag, but the lag correlations are skewed towards positive lags, which is a signature of temperature leading ozone anomalies by a small amount, similar to the annual cycle in Fig. 2.



235

Figure 4. Correlation of deseasonalized SHADOZ ozone and temperature time series as a function of height and time lag (in months). Positive lag denotes temperature leading ozone.

A scatter plot of the SHADOZ temperature vs. ozone deseasonalized anomalies at 24 km over 1998-2016 is shown in Fig. 5, highlighting the strong observed correlation. The slope of the (T/O₃) variations is near 6.1 (K/ppmv). This slope changes as a function of altitude (as shown below), and this is one of the quantities that we aim to understand from a simple perspective.

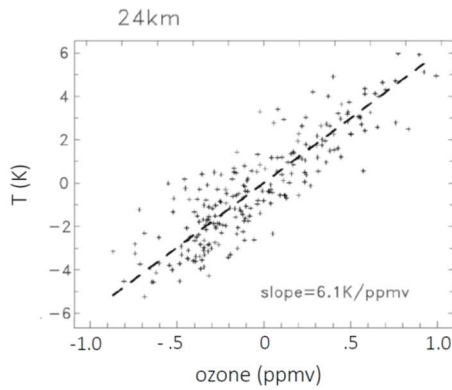


Figure 5. Scatter plot of deseasonalized temperature vs. ozone anomalies from SHADOZ data at 24 km (data as in Fig. 3).

245

4.2 Satellite observations

We use MLS and GPS satellite data to quantify ozone-temperature correlations over a continuous range of time scales from days to over a decade. Time series of zonal mean GPS temperatures and MLS ozone over the equator (10° N-S) at 24 km (31 hPa for MLS) are shown in Fig. 6, for pentad averages covering September 2004 – March 2018. Visual

250 inspection of Fig. 6 shows a clear signature of the QBO (as in Fig. 3), and strong correlations of ozone and temperature across all scales of variability, including both long- and short-term fluctuations.

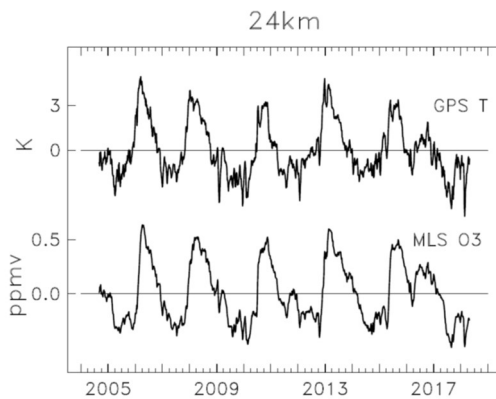


Figure 6. Time series of zonal average GPS temperatures and MLS ozone at 24 km, for averages over 10° N-S.

255 Power spectra for temperature and ozone at 24 km are shown in Fig. 7a. In these and the following spectral plots, the ordinate shows the wave period (from 10 to 4990 days) using a logarithmic frequency axis, in order to more clearly separate low- and high-frequency behaviour. The spectra for both quantities show most power at low frequencies, with peaks linked to the QBO, annual and semi-annual cycles. At altitudes below 24 km the annual cycle is more pronounced, while above 24 km the semi-annual cycle is larger. Power decreases systematically at periods shorter than semi-annual for both ozone and temperature in Fig. 7a. Temperature-ozone coherence squared (coh^2) at 24 km is shown in Fig. 7b, highlighting significant values over nearly the entire range of periods longer than ~ 20 days. There is a relative minimum in coh^2 near the semi-annual cycle, and this could possibly be related to the semi-annual variation in low-latitude ozone photochemical production noted above, which adds additional ozone variability that is less coherent with temperature. The reason for the lack of coherence at the shortest resolved time scales (< 20 days) is unknown, but could be related to very low power in both data sets (Fig. 7a) and poorer temporal resolution of these time scales based on pentad data. There is a relatively small phase difference between ozone and temperature over all frequencies, as shown below. Similar behavior is found for temperature-ozone coh^2 and phase for all altitudes over 17-27 km. Above 29 km there is a strong coh^2 maximum for the semi-annual oscillation (~ 180 days period), where ozone and temperature are approximately out of phase (not shown). This behavior is due to the transition to photochemical control of ozone and the impact of temperature on the odd-oxygen (O_x) loss rate
265
270 (Brasseur and Solomon, 2005).

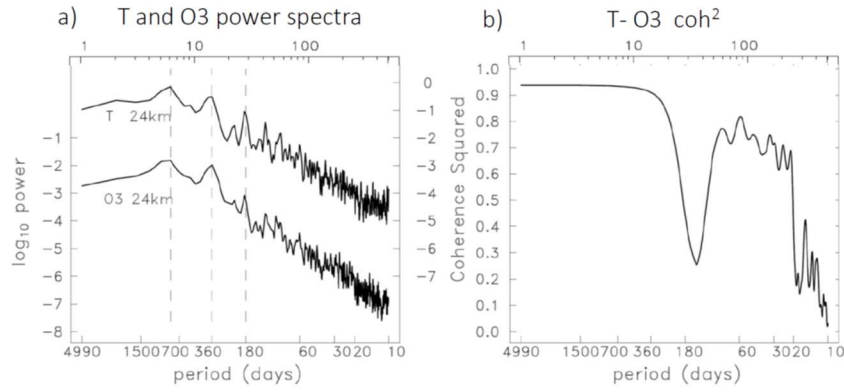


Figure 7. (a) Power spectra for GPS temperature and MLS ozone at 24 km as a function of wave period. Logarithmic power units are (K^2 – right axis) and (ppmv^2 – left axis). The vertical dashed lines identify peaks in the spectra associated with the QBO, annual and semi-annual cycles. Top logarithmic axis indicates the spectral estimates. b) Coherence squared between temperature and ozone at 24 km as a function of wave period.

275

5 Comparisons with idealized model calculations

We next compare frequency-dependent (X_σ/T_σ) amplitude and phase between observations and results from the idealized model calculations (Eqns. 9a-b). Figure 8a compares observed and modeled 24 km (T_σ/X_σ) amplitude as a function of frequency. Observations are based on the GPS temperature/MLS ozone results, where (T_σ/X_σ) is calculated from the respective harmonic coefficients and the ratio is smoothed in frequency. Model results are shown with and without including ozone damping effects, which has relatively small influence, along with calculations neglecting ozone feedback effects on temperature ($\beta=0$). Additionally, Fig. 8a includes the (T_σ/X_σ) ratio estimated from deseasonalized SHADOZ anomalies (from Fig. 5) which are mainly associated with the QBO (~ 28 months period). The observed (T_σ/X_σ) ratio shows a systematic change over the frequency range, with approximately a factor of two decrease in the ratio for low frequencies (periods > 150 days) compared to high frequencies. The idealized model results show a similar (T_σ/X_σ) frequency dependence, although with substantial disagreement on the detailed shape of the transition region between semi-annual and interannual (QBO) periods, with a slower transition in the model. This disagreement is not understood but might be related to the semi-annual ozone photochemical production term over the equator discussed above, which is not included in the model calculations. The overall systematic change with frequency in Fig. 8a corresponds to the change from ozone-temperature coupling via transport (high frequency) to radiative balance (low frequency). Including the ozone damping (δ) slightly improves the agreement at low frequencies.

285

Differences between the full model and $\beta=0$ results in Fig. 8a quantify the ozone feedback on temperature in the coupled system. Ozone radiative feedback is mainly important for low frequency ('slow') variability, and becomes increasingly important for the longest time scales. For example, for the QBO time period (28 months) the ozone feedback

295 increases the (T_{σ}/X_{σ}) ratio at 24 km by approximately 40%, with even larger effects at lower frequencies. We note this increasing importance of ozone feedbacks for low frequencies is consistent with the results of Charlesworth et al (2019).

The observed and modeled (T_{σ}/X_{σ}) phase relationship as a function of frequency is shown in Fig. 8b, showing approximately in-phase behavior across all frequencies in both cases. The model (T_{σ}/X_{σ}) phase is slightly positive (as expected from Section 3), and in approximate agreement with observed results. Similar behavior to Fig. 8 is found in the
 300 satellite data for all altitudes over 19-27 km. Neglect of ozone feedbacks ($\beta=0$) gives worse agreement with observations.

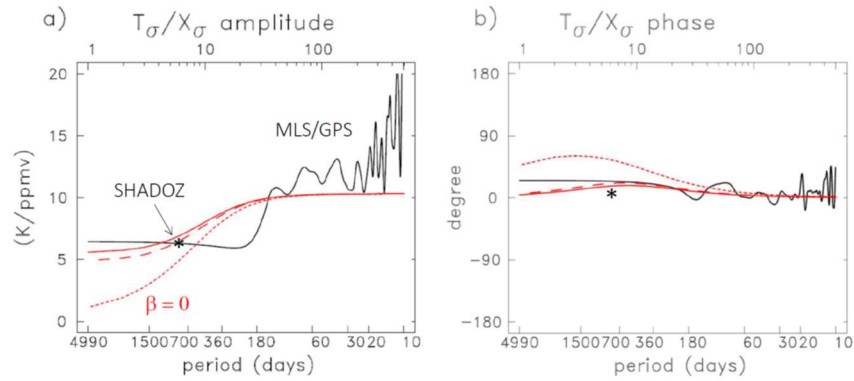
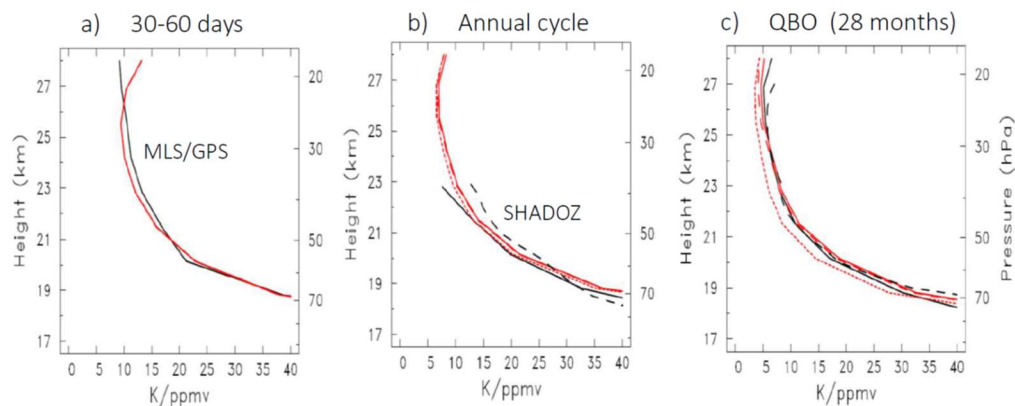


Figure 8. (a) (T_{σ}/X_{σ}) ratio at 24 km as a function of wave period. Black line shows observational results from MLS/GPS satellite data, and red lines show idealized model calculations (solid red line includes ozone damping, dashed red line is for $\delta=0$, and dotted red line is for $\beta=0$). The (T_{σ}/X_{σ}) ratio derived from deseasonalized SHADOZ data at 24 km (Fig. 5) is also shown, which is mainly associated with the QBO (~28 months period). (b) corresponding (T_{σ}/X_{σ}) phase differences.
 305

Vertical profiles of observed and modeled (T_{σ}/X_{σ}) amplitude are shown in Fig. 9 for three different frequency bands, corresponding to ‘fast’ frequencies (30-60 days period, Fig. 9a), annual cycle (Fig. 9b) and QBO (Fig. 9c). In addition to observations from the MLS/GPS data, we include the corresponding ratios calculated from SHADOZ ozone and temperature data for the annual cycle (e.g. Fig. 2a), calculated as the ratio of the respective ozone and temperature maximum-minimum values over the annual cycle, for altitudes 19-23 km where the annual cycle is distinct in the data. Figure 9c includes SHADOZ results for deseasonalized anomalies, which are mainly linked to the QBO, and derived from regression as in Fig. 5. These SHADOZ results in Figs. 9b-c agree well with the corresponding estimates from MLS/GPS satellite data. The fast frequencies (Fig. 9a) are governed by vertical transport with a (T_{σ}/X_{σ}) vertical profile close to (S/X_z) (Fig. 1c), and the model shows a good fit to the observed vertical structure, at least up to ~27 km. The annual cycle (Fig. 9b) is close to the cross-over between high- and low-frequency behavior, and the model again shows approximate agreement to observations over altitudes where the annual cycle is large (~19-23 km). This agreement helps confirm the interpretation that the annual cycles in tropical stratospheric temperature and ozone (e.g. Fig. 2) can be interpreted as coupled responses to the
 315

320 annual cycle in tropical upwelling, with ozone feeding back on temperature. For the lower frequency QBO variations (Fig. 9c) the idealized model shows good agreement with the (T_σ/X_σ) amplitude from both the satellite data and SHADOZ throughout the profile. Our conclusions from these comparisons is that the idealized model can quantitatively explain the observed (T_σ/X_σ) amplitude and phase relationships in the tropical lower stratosphere, including their dependence on frequency and altitude.



325

Figure 9. Vertical profiles of (T_σ/X_σ) amplitude for selected frequency bands. (a) 30-60 day periods, (b) annual cycle (12 months period), (c) QBO period (\sim 28 months). The solid black lines are results from MLS/GPS satellite data, and red lines show idealized model calculations (solid red line includes ozone damping, dashed red lines for $\delta=0$, and dotted red lines for $\beta=0$). Additionally, results from SHADOZ ozone and temperature data are included as dashed black lines in (b-c), as described in text. Observations for the annual cycle (b) are only shown over altitudes 19-23 km where the annual cycle is relatively large and distinct.

330

6 Summary and discussion

Observations show strong correlations between ozone and temperature in the tropical lower stratosphere, and calculations show that the ozone radiative feedbacks significantly enhance temperatures, e.g. by \sim 30% for the annual cycle (e.g. Ming et al, 2017). This ozone feedback significantly enhances thermal variability in global model simulations (Yook et al, 2020). The goals of this work include providing an update of observational evidence for T-O3 coupling and simplified understanding based on idealized zonal mean theory. The excellent long-term tropical ozonesonde measurements from SHADOZ demonstrate approximate in-phase T-O3 correlations for the annual cycle (Fig. 2) and for interannual anomalies (Figs. 3-5), which are dominated by the QBO. Long-term continuous satellite measurements from zonal average MLS and GPS data agree well with these results for annual and interannual variations, and furthermore demonstrate strong T-O3 coherence for faster sub-seasonal variability (Figs. 6-7b). This coherent behavior is observed throughout the lower to middle stratosphere, \sim 17-27 km, with T-O3 anomalies approximately in phase over all altitudes. A key result is that the observed $(T/O3)$ ratio changes as a function of frequency, with approximately half the ratio for low frequencies (annual cycle and

340

longer) compared to faster variability (Fig. 8a). The (T/O3) ratio also depends on altitude, with much larger ratios for levels in the lower stratosphere (Fig. 9). These are the key observational characteristics of T-O3 coupling that we seek to explain.

345 We compare observations to results from idealized zonal mean theory, assuming vertical advection from the upward Brewer-Dobson circulation controls thermal balances and ozone transport, i.e. neglecting mean meridional advection and eddy transport terms. This is a reasonable approximation in the tropical lower stratosphere above the TTL (Abalos et al, 2013), although eddy transport from monsoon circulations makes important contributions to ozone tendencies during boreal summer at and below ~18 km (Konopka et al, 2009, 2010; Stolarski et al, 2014). Thermodynamic balance includes linear radiative damping (α) and ozone feedback (β) terms, and the coupled equations (including linear ozone damping δ) can be
350 solved analytically to calculate the (T/O3) ratio as a function of frequency and altitude, dependent on model parameters α , β and δ and the ratio of background gradients expressed as (S/X_z). In general, ozone damping is a minor influence over most of the domain because of the long ozone lifetimes. The model balances highlight two time scales for T-O3 coupling, including ‘fast’ variability where the (T/O3) ratio is determined by the background vertical gradients (S/X_z) and ‘slow’ time
355 scales determined by radiative balance (β/α in the zero frequency limit). The idealized model shows a functional frequency dependence for the (T/O3) ratio similar to observations (Fig. 8a), although there is disagreement in the transition region where the observations show a more rapid (T/O3) transition with a slight minimum near the semiannual period. This detail is not well understood, but could be influenced by a semiannual ozone photochemical production term in the equatorial region related to solar inclination (Abalos et al, 2013) that is not included in our model, along with neglected eddy transport effects,
360 especially near the tropopause. This semi-annual ozone production may also explain the relative minimum in T-O3 coherence squared near this frequency found in Fig. 7b. The vertical profiles of (T/O3) ratio agree well with the observations for both fast (Fig. 9a) and slow (Figs. 9b-c) time scales, enhancing confidence in a simple understanding.

Ozone feedback on temperature is easy to quantify in our model by comparing results neglecting the feedback ($\beta=0$). Results show important ozone feedbacks for low frequency variations (i.e. the ‘slow’ regime), and the feedback
365 becomes increasingly important at lower frequencies (e.g. Fig. 8a). We note that the frequency-dependent T-O3 ozone feedback shown here is consistent with the results of Charlesworth et al (2019), which show larger ozone radiative impacts on tropopause temperatures for low frequencies.

One further aspect of coupled T-O3 behavior can be deduced from Eq. 3, noting that the α and β terms are closely coupled by observed T-O3 correlations in the lower stratosphere. Using the empirical approximation $\Delta X \sim \Delta T (X_z/S)$, where
370 $\Delta X = \beta (X - X_{eq})$ and likewise for ΔT , the combined terms ($-\alpha \Delta T + \beta \Delta X$) in Eq. 3 can be rewritten as ($-\alpha \Delta T + \beta' \Delta T$). These terms can be combined into $-\alpha_{eff} \Delta T$, with $\alpha_{eff} = (\alpha - \beta')$ representing an ‘effective’ thermal damping time scale combining both radiative relaxation and ozone feedback effects. Using realistic α and β' values (Fig. 1a), α_{eff} is significantly smaller than α alone, i.e. the ozone feedback increases the radiative damping time scale compared to radiative relaxation alone. This result is consistent with the effective timescales inferred by Fueglistaler et al. (2014) and with the coupled

375 chemistry-climate model calculations in Yook et al (2020), their Fig. 6. Alternatively, since the ozone-radiative feedback
arises primarily from transport effects, its effect can also be viewed as an enhancement to the dynamical heating.

It is worthwhile to appreciate the limitations associated with the idealized model calculations, especially
uncertainties related to the parameters α and β , which control the low frequency model behavior. While Hitchcock et al
(2010) show that linear regression on temperature captures $\sim 80\%$ of the variance in modeled radiative heating rates in the
380 tropical lower stratosphere, the broad spectrum of vertical scales in this region can introduce additional uncertainties in
estimating α . Our calculations of ozone heating via the β term in Eq. 3 neglects the effects of non-local ozone changes,
which will also depend in detail on the vertical scale of perturbations. In spite of these caveats, the overall agreement
between model and observations demonstrates that the idealized zonal mean theory (quantifying coupled T-O3 response to
variations in the Brewer-Dobson circulation) is a valid perspective to understand the strong T-O3 coupling in the real
385 atmosphere.

Acknowledgements

The National Center for Atmospheric Research is sponsored by the U.S. National Science Foundation. This work
has been partially supported by the COSMIC NSF-NASA Cooperative Agreement under Grant 1522830, and by the NASA
390 Aura Science Team under Grant 80NSSC20K0928. AM would like to acknowledge support from the Leverhulme Trust as
an early career fellow. We thank Marta Abalos, Rolando Garcia, Paul Konopka and Lan Luan for discussions and comments
that significantly improved the manuscript, and two anonymous reviewers for constructive reviews.

Data Availability

395 SHADOZ data were obtained from the SHADOZ website <https://tropo.gsfc.nasa.gov/shadoz/>. MLS ozone data were
obtained from <https://mls.jpl.nasa.gov/index-eos-mls.php>, and GPS temperatures were obtained from the COSMIC Data
Analysis and Archive Center (CDACC) website <https://cdaac-www.cosmic.ucar.edu/>.

Author contributions

400 The study was conceived by WJR, and data analysis was performed by FW. AM and PH provided input for the idealized
model calculations and contributed to interpretation of results. The paper was written by WJR, with editing from AM and
PH.

Competing interests

405 The authors declare that there are no competing interests.

References

- Abalos, M., Randel, W.J. and Serrano, E.: Variability in upwelling across the tropical tropopause and correlations with tracers in the lower stratosphere. *Atmos. Chem. Phys.*, 12, 11505–11517, doi:10.5194/acp-12-11505-2012, 2012.
- Abalos, M., Randel, W. J., Kinnison, D. E., and Serrano, E.: Quantifying tracer transport in the tropical lower stratosphere
410 using WACCM, *Atmos. Chem. Phys.*, 13, 10591–10607, doi:10.5194/acp-13-10591-2013, 2013.
- Andrews, D. G., Holton, J.R. and Leovy, C. B.: Middle Atmosphere Dynamics. Academic Press, 489 pp., 1987.
- Anthes, R.A., and coauthors: The COSMIC/FORMOSAT-3 Mission: Early results. *Bull. Am. Meteorol. Soc.*, 89, 313–333, 2008.
- Baldwin, M.P., Gray, L.J., Dunkerton, T.J., Hamilton, K., Haynes, P.H., Randel, W.J., Holton, J.R., et al.: The Quasi-
415 Biennial Oscillation. *Rev. Geophys.*, 39, 179–229, 2001.
- Birner, T., and Charlesworth, E. J.: On the relative importance of radiative and dynamical heating for tropical tropopause temperatures. *J. Geophys. Res. - Atmos.*, 122, 6782–6797. <https://doi.org/10.1002/2016JD026445>, 2017.
- Brasseur, G. and Solomon, S.: Aeronomy of the Middle Atmosphere. Springer, 644 pp, doi:10.1007/1-4020-3824-0, 2005.
420
- Calvo, N., García, R.R., Randel, W.J. and Marsh, D.R.: Dynamical mechanism for the increase in tropical upwelling in the lowermost tropical stratosphere during warm ENSO events. *J. Atmos. Sci.*, 67, 2331–2340, doi:10.1175/2010JAS3433.1, 2010.
- 425 Chae, J. H., and Sherwood, S.C.: Annual temperature cycle of the tropical tropopause: A simple model study, *J. Geophys. Res.*, 112, D19111, doi:10.1029/2006JD007956, 2007.
- Charlesworth, E. J., Birner, T., & Albers, J. R.: Ozone transport-radiation feedbacks in the tropical tropopause layer. *Geophys. Res. Lett.*, 46. <https://doi.org/10.1029/2019GL084679>, 2019.
- 430 Chipperfield, M. P. & Gray, L. J.: Two-dimensional model studies of the interannual variability of trace gases in the middle atmosphere. *J. Geophys. Res.*, 97(D5), 5963–5980. <https://doi.org/10.1029/92JD00029>, 1992.
- Dacie, S., Kluft, L., Schmidt, H., Stevens, B., Buehler, S. A., Nowack, P. J., et al.: A 1D RCE study of factor affecting the tropical tropopause layer and surface climate. *J. Clim.*, 32, 6769–6782. <https://doi.org/10.1175/JCLI-D-18-0778.1>,
435 2019.
- Diallo, M., Riese, M., Birner, T., Konopka, P., Müller, R., Hegglin, M. I., Santee, M. L., Baldwin, M., Legras, B., and Ploeger, F.: Response of stratospheric water vapor and ozone to the unusual timing of El Niño and the QBO disruption in 2015–2016, *Atmos. Chem. Phys.*, 18, 13 055–13 073, <https://doi.org/10.5194/acp-18-13055-2018>,
440 2018.
- Forster, P. M., G. Bodeker, R. Schofield, S. Solomon, and D. Thompson: Effects of ozone cooling in the tropical lower stratosphere and upper troposphere, *Geophys. Res. Lett.*, 34, L23813, doi:10.1029/2007GL031994, 2007.
- 445 Fueglistaler, S., Haynes, P. H., & Forster, P. M.: The annual cycle in lower stratospheric temperatures revisited. *Atmos. Chem. Phys.*, 11, 3701–3711. <https://doi.org/10.5194/acp-11-3701-2011>, 2011.

- 450 Fueglistaler, S., Abalos, M., Flannaghan, T. J., Lin, P., and Randel, W. J.: Variability and trends in dynamical forcing of tropical lower stratospheric temperatures, *Atmos. Chem. Phys.*, 14, 13439–13453, <https://doi.org/10.5194/acp-14-13439-2014>, 2014.
- Gilford, D. M., Solomon, S., and Portmann, R.W.: Radiative impacts of the 2011 abrupt drops in water vapor and ozone in the tropical tropopause layer. *J. Clim.*, 29, 595–612, doi:10.1175/JCLI-D-15-0167.1, 2016.
- 455 Gilford, D. and Solomon, S.: Radiative effects of stratospheric seasonal cycles in the tropical upper troposphere and lower stratosphere. *J. Clim.*, 30, doi:10.1175/JCLI-D-16-0633.1, 2017.
- Hartmann, D.L., Holton, J.R. and Fu, Q.: The heat balance of the tropical tropopause, cirrus and stratospheric dehydration. *Geophys. Res. Lett.* 28, 1969-1972, 2001.
- 460 Hasebe, F.: Quasi-biennial oscillations of ozone and diabatic circulation in the equatorial stratosphere. *J. Atmos. Sci.*, [https://doi.org/10.1175/1520-0469\(1994\)051<0729:QBOOOA>2.0.CO;2](https://doi.org/10.1175/1520-0469(1994)051<0729:QBOOOA>2.0.CO;2), 1994.
- 465 Hauchecorne, A., Bertaux, J. L., Dalaudier, F., Keckhut, P., Lemennais, P., Bekki, S., Marchand, M., Lebrun, J. C., Kyrölä, E., Tamminen, J., Sofieva, V., Fussen, D., Vanhellemont, F., Fanton d'Andon, O., Barrot, G., Blanot, L., Fehr, T., and Saavedra de Miguel, L.: Response of tropical stratospheric O₃, NO₂ and NO₃ to the equatorial Quasi-Biennial Oscillation and to temperature as seen from GOMOS/ENVISAT, *Atmos. Chem. Phys.*, 10, 8873–8879, <https://doi.org/10.5194/acp-10-8873-2010>, 2010.
- 470 Hitchcock, P., Shepherd, T. G., & Yoden, S.: On the approximation of local and linear radiative damping in the middle atmosphere. *J. Atmos. Sci.*, 67, 2070–2085. <https://doi.org/10.1175/2009JAS3286.1>, 2010.
- Jenkins, G. M., and D. G. Watts: *Spectral Analysis and Its Applications*. Holden-Day, 525 pp., 1968.
- 475 Konopka, P., J. Grooß, F. Ploeger, and R. Müller: Annual cycle of horizontal in-mixing into the lower tropical stratosphere, *J. Geophys. Res.*, 114, D19111, doi:10.1029/2009JD011955, 2009.
- Konopka, P., J.-U. Grooß, G. Günther, F. Ploeger, R. Pommrich, R. Müller, and N. Livesey: Annual cycle of ozone at and above the tropical tropopause: Observations versus simulations with the Chemical Lagrangian Model of the Stratosphere (CLaMS), *Atmos. Chem. Phys.*, 10(1), 121–132, 2010.
- 480 Livesey, N. J., Read, W. G., Wagner, P. A., Froidevaux, L., Lambert, A., Manney, G. L., et al.: Aura Microwave Limb Sounder (MLS) version 4.2x level 2 data quality and description document. Tech. Rep., Jet Propulsion Laboratory. Retrieved from <http://mls.jpl.nasa.gov/>, 2018.
- 485 Marsh, D., Mills, M., Kinnison, D. E., & Lamarque, J. -F.: Climate change from 1850 to 2005 simulated in CESM1(WACCM). *J. Clim.*, 26, 7372-7391. doi:10.1175/JCLI-D-12-00558.1, 2013.
- 490 Ming, A., Maycock, A. C., Hitchcock, P., & Haynes, P.: The radiative role of ozone and water vapour in the annual temperature cycle in the tropical tropopause layer. *Atmos. Chem. Phys.*, 17, 5677–5701. <https://doi.org/10.5194/acp-17-5677-2017>, 2017.
- Morcrette, J.-J.: Radiation and cloud radiative properties in the European Centre for Medium Range Weather Forecasts forecasting system. *J. Geophys. Res. - Atmos.*, 96, 9121–9132, doi:10.1029/89JD01597, 1991.
- 495 Newman, P.A., and Rosenfield, J. E.: Stratospheric thermal damping times. *Geophys. Res. Lett.*, 24, 433-436, 1997.

- Park, M., Randel, W. J., Kinnison, D. E., Bourassa, A. E., Degenstein, D. A., Roth, C. Z., McLinden, C.A., Sioris, C.E., Livesey, N.E, and Santee, M. L.: Variability of stratospheric reactive nitrogen and ozone related to the QBO. *J. Geophys. Res.*, 122, <https://doi.org/10.1002/2017JD027061>, 2017.
- 500 Polvani, L. M. and Solomon, S.: The signature of ozone depletion on tropical temperature trends, as revealed by their seasonal cycle in model integrations with single forcings, *J. Geophys. Res.*, 117, D17102, doi:10.1029/2012JD017719, 2012.
- Randel, W.J., Park, M., Wu, F. and Livesey, N.: A large annual cycle in ozone above the tropical tropopause linked to the Brewer-Dobson circulation. *J. Atmos. Sci.*, 64, 4479-4488, 2007.
- 505 Randel, W.J., Garcia, R.R., Calvo, N. and Marsh, D.: ENSO influence on zonal mean temperature and ozone in the tropical lower stratosphere. *Geophys. Res. Lett.*, 36, L15822, doi:10.1029/2009GL039343, 2009.
- Randel, W.J., and Thompson, A.M.: Interannual variability and trends in tropical ozone derived from SAGE II satellite data and SHADOZ ozonesondes. *J. Geophys. Res.*, 116, D07303, doi:10.1029/2010JD015195, 2011.
- Randel, W.J. and Wu, F.: Variability of zonal mean tropical temperatures derived from a decade of GPS radio occultation data. *J. Atmos. Sci.*, 72, 1261-1275, doi:10.1175/JAS-D-14-0216.1, 2015.
- 510 Stolarski, R. S., Waugh, D.W., Wang, L., Oman, L.D., Douglass, A.R. and Newman, P.A.: Seasonal variation of ozone in the tropical lower stratosphere: Southern tropics are different from northern tropics, *J. Geophys. Res. - Atmos.*, 119, 6196–6206, doi:10.1002/2013JD021294, 2014.
- Thompson, Anne M. et al.: Southern Hemisphere Additional Ozonesondes (SHADOZ) 1998–2000 tropical ozone climatology: 1. Comparison with Total Ozone Mapping Spectrometer (TOMS) and ground-based measurements. *J. Geophys. Res. - Atmos.*, 108(D2), 8238, 10.1029/2001JD000967, 2003.
- 515 Thompson, A. M., Witte, J.C., Sterling, C., Jordan, A., Johnson, B.J., Oltmans, S.J., ... Thiongo, K.: First reprocessing of Southern Hemisphere Additional Ozonesondes (SHADOZ) ozone profiles (1998-2016): 2. Comparisons with satellites and ground-based instruments. *J. Geophys. Res. - Atmos.*, 122, 13,000-13,025. <https://doi.org/10.1002/2017JD027406>, 2017.
- 520 Thuburn, J., & Craig, G. C.: On the temperature structure of the tropical stratosphere. *J. Geophys. Res.*, 107, 4017. <https://doi.org/10.1029/2001JD000448>, 2002.
- Tweedy, O.V., Waugh, D.W., Stolarski, R.S., Oman, L.D., Randel, W.J. and Abalos, M.: Hemispheric differences in the annual cycle of tropical lower stratospheric transport and tracers. *J. Geophys. Res. - Atmos.*, 122, 7183–7199, doi:10.1002/2017JD026482, 2017.
- 525 Witte, J. C., Schoeberl, M. R., Douglass, A. R., and Thompson, A. M.: The Quasi-biennial Oscillation and annual variations in tropical ozone from SHADOZ and HALOE, *Atmos. Chem. Phys.*, 8, 3929–3936, <https://doi.org/10.5194/acp-8-3929-2008>, 2008.

- 530 Witte, J.C., Thompson, A.M., Smit, H.G.J., Fujiwara, M., Posny, F., Coetzee, G.J.R., ... da Silva, F.R.: First reprocessing of
Southern Hemisphere ADditional OZonesondes (SHADOZ) profile records (1998-2015): 1. Methodology and
evaluation, *J. Geophys. Res. - Atmos.*, 122, 6611-6636. <https://doi.org/10.1002/2016JD026403>, 2017.
- Yook, S., D. W. J. Thompson, S. Solomon, and S.-Y. Kim: The key role of coupled chemistry-climate interactions in tropical
stratospheric temperature variability. *J. Clim.*, 33, 7619-7629, 2020.
- 535 Zhong, W. and Haigh, J. D. Improved Broadband Emissivity Parameterization for Water Vapor Cooling Rate Calculations,
J. Atmos. Sci., 52, 124–138, 1995.